(2)

Rotor/Body Aerodynamic Interactions

Mark D. Betzina, Charles A. Smith and Patrick Shinoda

October 1983

National Aeronautics and Space Administration

United States Army Aviation Research and Development Command

Rotor/Body Aerodynamic Interactions

Mark D. Betzina and Charles A. Smith, Ames Research Center, Moffett Field, California
Patrick Shinoda, Aeromechanics Laboratory, Research and Technology Laboratories,
U. S. Army Aviation Research and Development Command
Ames Research Center, Moffett Field, California

NASA
National Aeronautics and Space Administration
Ames Research Center
Moffett Field, California 94035

United States Army
Aviation Research and Development Command
St. Louis, Missouri 63166

ROTOR/BODY AERODYNAMIC INTERACTIONS

Mark D. Betzina and Charles A. Smith

NASA Ames Research Center
Moffett Field, California 94035 U.S.A.

and

Patrick Shinoda

Aeromechanics Laboratory
U.S. Army Research and Technology Laboratories (AVRADCOM)
Ames Research Center
Moffett Field, California 94035 U.S.A.

Abstract

A wind-tunnel investigation was conducted in which independent, steady-state aerodynamic forces and moments were measured on a 2.24-m-diam, two-bladed helicopter rotor and on several different bodies. The objective was to determine the mutual interaction effects for variations in velocity, thrust, tip-path-plane angle of attack, body angle of attack, rotor/body position, and body geometry. The results of the investigation show that the body longitudinal aerodynamic characteristics are significantly affected by the presence of a rotor and hub, and that the hub interference may be a major part of such interaction. This report presents the effects of various parameters on the interactions and discusses the difficulties encountered in determining the effect of the body on the rotor performance. Also discussed are plans for future research into this subject.

Nomenclature

A = rotor disk area, πR^2, m^2

b = number of rotor blades

c = rotor-blade chord, m

C_{D_B} = body wind-axis drag coefficient, D_B/qS_B

C_{L_B} = body wind-axis lift coefficient, L_B/qS_B

C_{M_B} = body wind-axis pitching moment coefficient, M_B/qS_B

C_P = body surface pressure coefficient, $(P - P_\infty)/q$

C_T = rotor thrust coefficient, $T/\rho(\Omega R)^2 A$

d = maximum body diam, m

D_B = body wind-axis drag, N

ℓ = body length, m

L_B = body wind-axis lift, N

M_B = body wind-axis pitching moment, N-m

P = local static pressure, Pa

P_∞ = free-stream static pressure, Pa

q = free-stream dynamic pressure, Pa

R = rotor radius, m

S_B = body maximum cross-sectional area, $\pi d^2/4$, m^2

T = rotor thrust (tip-path-plane axis), N

V = free-stream velocity, m/sec

X = longitudinal distance from hub center to body nose leading edge, m

X_B = longitudinal body coordinate, measured from body nose, positive downstream, m

Z = vertical distance from hub center to body centerline, m

α_B = body geometric angle of attack, positive nose up, deg

α_{TPP} = rotor geometric tip-path-plane angle of attack, positive for leading edge of plane up, deg

$\Delta( )$ = change in quantity due to interference

μ = advance ratio, $V/\Omega R$

ρ = free-stream air density, kg/m^3

σ = rotor solidity, $bc/\pi R$

Ω = rotor rotational speed, rad/sec

1. Introduction

Current analytical techniques permit reasonable predictions of the aerodynamic flow field around an isolated rotor or fuselage. However, the many components involved in a helicopter produce a flow field that is influenced not only by each component, but also by their mutual interactions. For example, a rotor wake may change fuselage characteristics, and the blockage caused by the fuselage could alter the nature of the rotor wake generation. Thus, the individual

components of a helicopter are highly coupled, and the aerodynamic characteristics depend on the entire helicopter system. This interacting flow field is difficult to model analytically because the present understanding of the detailed phenomena responsible for the interactions is incomplete. Current analytical techniques are not adequate to provide accurate performance, loads, vibration, and noise predictions for a complete helicopter system.

Configuration parameters, such as rotor/fuselage vertical separation, can affect the aerodynamic interactions in a manner which significantly changes performance, loads, or vibration. For example, Ref. [1] describes interactional aerodynamics problems that occurred during the YUH-61A UTTAS helicopter development program. The rotor/fuselage vertical separation was initially constrained because of a design requirement limiting the height of the helicopter. Because of encountering unexpectedly high dynamic loads, the rotor was subsequently raised to alleviate the problems.

Wind-tunnel tests of full-scale helicopter rotors have typically used a body of revolution to enclose the drive motors and transmission. Rotor characteristics have been obtained by simply subtracting the measured aerodynamic characteristics of the isolated body and hub from the total measured rotor performance. This approach neglects the mutual aerodynamic interactions between the rotor and body, and yields rotor performance in the presence of the body rather than isolated rotor performance which would provide valuable validation data for analyses. If these interactions could be determined, more accurate measurements of isolated rotor performance could be obtained.

A number of recent investigations have studied various aspects of the helicopter aerodynamic interaction problem. References [1] and [2] describe an extensive test that concentrated on the dynamic interactions affecting blade loads and fuselage vibration. References [3]-[5] describe investigations in which time-averaged fuselage surface pressures were measured for various configurations of rotors and bodies. Some success has been achieved in analytically predicting time-averaged surface pressures at an advance ratio of 0.05 (Ref. [5]). Reference [6] presents the effects of fuselage configuration on rotor loads. Reference [7] describes an experimental investigation of main rotor/tail rotor interactions in hover. Reference [8] describes an experimental investigation of main rotor/fuselage/tail rotor interactions in hover.

Experimental investigations were recently completed in the Ames 7- by 10-Foot Wind Tunnel to learn more about rotor/body aerodynamic interactions and the effects they have on steady-state body aerodynamic characteristics and rotor performance. (Although dynamic interactions affecting blade loads, fuselage vibration, and noise are important considerations, they are not addressed in this paper.) The bodies were 1/6-scale models of test modules used for testing full-scale rotors in the Ames 40- by 80-Foot Wind Tunnel. They provided basic shapes that are more easily modeled analytically than an actual helicopter fuselage, and allowed the study of configurations currently in use at Ames for testing full-scale rotors.

These investigations provided an extensive data base for the development and validation of analytical techniques. Some of the results are presented in Refs. [9] and [10]. This paper summarizes the most significant results and describes plans for future research on this subject. A complete set of data will be published in Ref. [11].

2. Experimental Investigation

Model Description

A simplified, small-scale helicopter system, consisting of a teetering, two-bladed rotor and a body of revolution (circular cross section), was used for these investigations. The 2.235-m-diam rotor blades were aerodynamically scaled to 1/6-scale AH-1G Cobra helicopter blades. The blades were not scaled dynamically, and had a relatively high stiffness when compared with full-scale blades. The characteristics of the rotor are shown in Table 1. The hub, which was not scaled, had a diameter equal to 14% of the rotor diameter.

Three bodies were tested as shown in Fig. 1. Bodies B_1 and B_2 were 1/6-scale models of test modules used for testing full-scale rotors in the Ames 40- by 80-Foot Wind Tunnel. The full-scale version of body B_1 is shown in Fig. 2. The models did not include the strut attachment fairings and hub cutout which exist on the full-scale modules. Body B_2E was an extended version of body B_2. It had nose and tail shapes identical to body B_2 but incorporated a cylindrical extension.

The rotor and body were mounted independently on separate balance systems in the Ames 7- by 10-Foot Wind Tunnel. The rotor forces and moments were measured on the wind-tunnel balance system; the body forces and moments were measured on an internal six-component strain-gage balance. There was no physical connection between the body and the rotor system; the normal rotor shaft between the fuselage and hub was not simulated. A symmetric airfoil fairing (not on the balance) shielded the rotor drive shaft from the wind. However, the controls and swashplate were exposed to the airstream and contributed to the measured rotor forces and moments. The data were corrected for this (as discussed below). The installation in the wind tunnel is shown in Figs. 3 and 4.

Bodies B_2 and B_2E were instrumented with static pressure taps along the upper surface centerline and in rings around the body at several longitudinal stations. Time-averaged surface pressures were recorded.

Complete descriptions of the test equipment used will be published in Ref. [11].

Test Procedure

Data were obtained for the isolated body, isolated rotor, and combined rotor/body configurations over the range of test parameters shown in Table 2. Data were not obtained at specific trim flight

conditions. However, the range of thrust and tip-path-plane angles encompasses typical trim conditions at each velocity. The parameters used to define body position are shown in Fig. 4. The baseline positions shown in Table 2 correspond to the full-scale test modules.

Each individual test run consisted of a sequence of rotor thrust levels while maintaining advance ratio, tip Mach number, and tip-path-plane angle of attack. Orientation of the rotor tip-path plane was held constant using cyclic pitch control while thrust was varied using collective pitch control. Advance ratio was varied by changing free-stream velocity. When body angle of attack was varied, body position was adjusted to maintain the position of the hub relative to the body. The rotor shaft angle was not varied.

Angles of attack were defined with standard sign conventions; a free-stream velocity in the direction shown in Fig. 4 resulted in positive angles of attack for both the body and the rotor tip-path plane. The wind-tunnel walls produce an effective change in angle of attack which is proportional to the rotor lift. The angle of attack correction, obtained from the method used in Ref. [12], was calculated as follows:

$$\Delta\alpha = 1.084 L_R/q \qquad (1)$$

where $\Delta\alpha$ is the angle-of-attack change (deg), L_R is the rotor lift (N), and q is the free-stream dynamic pressure (Pa). The data for both the rotor and body were computed in the corrected wind axis system. However, the rotor and body orientation were not adjusted to maintain a constant corrected angle of attack. Therefore, the angles of attack for the body and tip-path-plane indicated in Figs. 5-27 are the geometric angles in the wind tunnel.

Interaction Measurements

The objective of this investigation was to determine the interaction of both the rotor on the body aerodynamic characteristics and the body on the rotor performance. Data were obtained for the isolated body, body/hub, body/hub/rotor, hub/rotor, and isolated hub configurations. Table 3 shows the components of the forces and moments measured by each balance system for each configuration. For example, in the body/hub configuration, the wind-tunnel balance measures the sum of the isolated hub and the interference on the hub due to the presence of the body (H + H/B); the body balance measures the sum of the isolated body and the interference on the body due to the presence of the hub (B + B/H). (It should be noted that the hub referred to here includes the rotor hub, swashplate, controls, and the portion of the drive shaft extending from the fairing; see Fig. 3.)

The total interaction of the rotor and hub on the body, B/HR, can be determined by subtracting the isolated body data from that in the body/hub/rotor configuration. The interaction of the hub on the body in the body/hub configuration, B/H, can be similarly determined. However, since the interaction of the hub on the body is likely to change when the rotor is present, it is not possible to determine the interaction of only the rotor blades on the body (B/HR $\neq$ B/H + B/R).

Similarly, because the hub and rotor loads cannot be separated, the interaction of the body on the rotor performance, R/B, cannot be separated from a change in the interaction of the body on the hub and controls. Rotor performance data were obtained by subtracting the measured loads in the isolated hub configuration or the body/hub configuration from the measured rotor loads in the hub/rotor or body/hub/rotor configuration, respectively. However, since the hub loads change in the presence of the rotor, the rotor performance includes these changes.

3. Results and Discussion

Effect of Rotor on Body

Body aerodynamic characteristics were measured for the isolated body, body/hub, and body/hub/rotor configurations. The aerodynamic loads on the hub and rotor are not included in the measured body loads because the hub and rotor are not physically connected to the body. However, the interference effects caused by the presence of the hub and rotor are included in the measured body data.

These interference effects on body B_2 in the baseline configuration are shown in Fig. 5 for an advance ratio of 0.3 and a moderate thrust coefficient. Body lift, drag, and pitching moment were computed in the wind-axis system as shown in Fig. 4. The body coefficients shown were normalized by free-stream dynamic pressure and maximum cross-sectional area of the body. The body length was used to normalize the pitching moment. The moment center was located as shown in Fig. 1; it corresponds to the longitudinal position of the rotor hub in the baseline configuration. The presence of the hub and rotor causes large changes in body lift, drag, and pitching moment. However, the interference effect of the hub on the body without the rotor blades is nearly as large as the total hub/rotor effect. Similar results were obtained for the other bodies.

Because the hub interference may be modified when subjected to the rotor wake, it is impossible to separate the rotor interference from the hub interference in the hub/rotor configuration. It appears, however, that the hub may be responsible for a major part of the rotor/hub interference on the body. This is confirmed by looking at the pressure distribution on the body upper surface along the longitudinal centerline (Fig. 6). These data are for the same three configurations shown in Fig. 5. The longitudinal position of the hub is about 20% of the body length, extending from approximately 6% to about 34%. The hub causes a region of lower pressure immediately behind it and a moderately reduced pressure on the remaining aft portion of the body. This contributes to the increased lift and negative pitching moment indicated in Fig. 5. It also creates a region of higher pressure forward of the hub which also contributes to the negative pitching moment. These data imply a blockage effect where the lower momentum in the hub wake induces an acceleration of the flow in the region between the hub wake and the body. (If a rotor shaft between the body and hub had been included, this result might have been different.) The addition of the rotor seems to accentuate the

hub effect in the region near the hub while only producing a small increase in surface pressure on the aft portion of the body.

To show the effect of rotor thrust, the body coefficients were plotted vs the rotor thrust coefficient. Figure 7 shows the results for body B_2 in the baseline position. Note that the body lift increases with thrust while the drag decreases. This is most pronounced at the lowest advance ratio, 0.15. Similar trends were obtained with the other bodies. The effect of rotor thrust on the body surface pressure distribution along the longitudinal centerline is shown in Fig. 8 for an advance ratio of 0.15. Again, the region immediately behind the hub contributes to the increased lift at the higher thrust. Also note that the lower surface pressure increases, implying a general stagnation of the flow around the body near the rotor wake (which might also be responsible for the slight drag reduction shown in Fig. 7). For the high thrust case shown in Fig. 8, the large pressure variations on the aft upper surface may result from the tip vortex interaction with the body.

To assess the significance of these interactions, it is helpful to compare their magnitudes with the rotor thrust. Figure 9 shows the body forces and moments normalized by thrust plotted vs rotor thrust coefficient for body B_2 in the baseline position. At an advance ratio of 0.15, the body forces and moments are very small compared with the rotor thrust. However, they increase with advance ratio as the free-stream velocity becomes large relative to the wake velocity.

Clearly, the body forces and moments are a function of both free-stream dynamic pressure and rotor thrust. An appropriate non-dimensional parameter is the ratio of the free-stream dynamic pressure to the rotor disk loading, which is simply the inverse of a rotor thrust coefficient normalized by the free-stream velocity instead of the tip speed. This parameter, a measure of the gross behavior of the flow field, is related to the velocity ratio used in Ref. [10] as follows:

$$\frac{q}{T/A} = \frac{1}{4}\left(\frac{V}{V_h}\right)^2 \qquad (2)$$

where $V_h = (T/2\rho A)^{1/2}$. The data from Fig. 9 are plotted vs this parameter in Fig. 10. The data for all four advance ratios collapse onto a nearly linear single line. Looking closely at the data points shown in Fig. 10, it appears that there is still a small effect of advance ratio at any given ratio of free-stream dynamic pressure to disk loading. However, for constant body angle of attack, the dynamic pressure to disk loading ratio is clearly the primary parameter determining the body characteristics.

Also shown in Fig. 10 are dashed lines indicating constant body coefficients (normalized by free-stream velocity). Note that large changes in C_{L_B}, C_{D_B}, and C_{M_B} can occur at small values of the dynamic pressure to disk loading ratio without a singificant effect relative to the rotor thrust.

The body lift was positive for all cases shown in Fig. 10 ($\alpha_B = 0°$). If the body had some horizontal surfaces, such as a wing or tail, the rotor might produce downward forces on these surfaces larger than the upward forces generated on the body, resulting in net negative lift. It was not possible to obtain hover or very low velocity data in the wind tunnel because of the large wall effects at low speeds. Since the body lift in hover (out of ground effect) must be negative, it appears that there is a transition region (at speeds below those tested in these investigations), where the rotor wake engulfs the body and the lift force reverses sign. It is possible, however, that the lift data shown in Fig. 10 at very low speed are being influenced by a ground effect in the wind tunnel, causing the lift curve to approach a positive value at hover. Very low speed data out of ground effect would be required to completely define the loads in this region.

Figures 11-13 present comparisons between bodies B_1 and B_2 in their baseline positions. The curve shown is a second order polynomial curve fit of the measured data (see Fig. 10 for the B_2 data). The standard deviation of the data from the curve is indicated. This standard deviation includes both scatter and the effect of advance ratio as discussed above. As shown in Fig. 1, the bodies are quite different from each other in size and shape. The longitudinal position of the hub for the baseline position corresponds with the location of the moment center shown in Fig. 1. Body B_1 extends much farther both forward and aft of the hub than body B_2.

Figure 11 shows the effect of body configuration on body lift. Body B_2 produces more lift than body B_1 but the trends are similar. Recall from Figs. 6 and 8 that the lift on body B_2 resulted from the effect of the hub on the area immediately behind the hub and that the forward part of the body had a negative lift contribution. Surface pressure data for body B_1 are not available, but it appears that the increased body length forward of the hub reduces the net lift. Figures 12 and 13 show the effect of body configuration on body drag and pitching moment, respectively. The pitching moment (normalized by body length) and the drag are nearly identical for the two bodies.

The effects of rotor tip-path-plane angle of attack on body B_2 forces and moments are shown in Figs. 14-16. As the rotor tip-path plane is tilted forward from 0° to -8°, there is a substantial increase in body lift accompanied by a small drag reduction and a slightly more negative pitching moment. As the rotor tip-path-plane angle varies, the vertical position of the rotor wake changes substantially relative to the body. As the rotor wake approaches the body, or impinges on a larger portion of the body, the body lift increases. This may result from an interaction of the rotor wake with the hub wake. Figure 17 shows that the lift and pitching moment trends with rotor tip-path-plane angle are similar for the various bodies tested. The drag trend, however, is inconclusive.

To investigate further the effect of rotor-wake position relative to the body, the vertical separation between the rotor and body was varied. The results for body B_2 are shown in Figs. 18-20. Consistent with the trend observed with changes in rotor tip-path-plane

angle, the body lift increases and the pitching moment becomes more negative as the vertical separation is reduced. The drag trend remains inconclusive. However, these results include the effect of changing the position of the hub wake in addition to the effect of the rotor-wake position.

Figure 21 shows the effect of vertical separation on the hub and rotor interference. The hub interference was determined by subtracting the isolated body data from the body data obtained in the presence of the hub with rotor blades removed. The total hub and rotor interference was obtained by subtracting the isolated body data from the body data obtained in the presence of the operating rotor and hub. The trend of the hub interference with separation distance is very similar to the trend observed for the total hub/rotor interference. This indicates that the position of the hub wake may be responsible for a major part of the observed trends with vertical separation distance.

Further insight into the hub and rotor interference effects on the body is gained by examining them for various body angles of attack and velocities. Figure 22 shows the interference lift, drag, and pitching moment on body B_2. The presence of the hub produces a positive change in body lift and drag proportional to the free-stream dynamic pressure. The negative change in pitching moment resulting from the hub's presence is also proportional to free-stream dynamic pressure. When the rotor blades are added, the trend remains linear with dynamic pressure but there is a constant component as well as a slope change. This can be viewed as a thrust effect, independent of velocity, plus a hub effect that is slightly changed from the blades-off case. Also note that the hub interference becomes a larger percentage of the total rotor/hub interference as velocity increases. Therefore, it appears that the hub interference is particularly important at high speeds where it may be the major source of the interference.

The effect of body angle of attack on the hub and rotor interference effects is shown in Fig. 23 for bodies B_1 and B_2 at a velocity of 60 m/sec. The trends for the hub interference are very similar to those for the total hub and rotor interference. This indicates that the effect of body angle of attack may be primarily a result of the hub interference. The lift and pitching moment interference is more sensitive to body angle of attack for the longer body, B_1, than it is for the shorter body, B_2. It is believed that the longer tail on body B_1 moves into the hub wake at negative angles of attack so that the accelerated flow region between the hub wake and body disappears. The hub wake remains separated from body B_2 for the angles of attack shown because of the shorter tail.

The effects of body longitudinal position are shown in Figs. 24-26. A large decrease in body lift and a large increase in body drag occur along with a large negative shift in pitching moment when body B_2 is moved forward relative to the rotor by 20% of the rotor radius. To help explain this, the characteristics of body B_2E are also shown. Body B_2E has the same nose and tail shape as body B_2 with a cylindrical extension added in the middle. It was installed

such that the nose was at the same position as body B_2 in the forward position, and the tail was at the same position as body B_2 in the aft position. By comparing the results for body B_2 in the aft position with body B_2E, the effect of the nose position can be observed, and when in the forward position, the effect of the tail position can be observed. The majority of the lift change results from the change in tail position, whereas the majority of the drag change results from the change in nose position. The location of the moment center used for the pitching moment shown was the longitudinal location of the hub for body B_2E and body B_2 in the aft position. The moment center remained fixed relative to the body when body B_2 was moved to the forward position.

Figure 27 shows the effect of body longitudinal position on the hub and rotor interference. It appears that the effect of body longitudinal position on body lift may primarily result from the hub interference and that the hub interference is an important part of the effects on drag and pitching moment. Also note that the constant term (thrust effect) in the body interference lift seems to be independent of body longitudinal position.

There are several differences between the experimental configuration and a realistic helicopter that may have significant effects on the interference of the rotor/hub on the body. Because of structural requirements, the hub was larger than an appropriately scaled one and included relatively large controls and swashplate located on the inflow side of the rotor disk. Also, because a rotor shaft was not simulated, the flow between the hub and body was unobstructed. Therefore, the magnitude of the hub effect may not be indicative of full-scale results. However, it is believed that the effect of the hub on the body is very significant and should be included in analytical techniques for predicting rotor/body interactions.

The full-scale versions of body B_1 and B_2 are used for wind-tunnel testing of full-scale rotor systems. Changes in the body forces and moments due to the presence of the rotor will affect the measured rotor performance. The interference effects of the rotor/hub on the body observed in these investigations indicate that these effects must be considered when determining full-scale rotor performance.

Effect of Body on Rotor

As discussed above, there are several unmeasured effects that cannot be separated from the desired interaction effects. In addition to the interaction of the body on the rotor, there is the change in the interaction of the body on the hub/controls due to the presence of the rotor, the change in the interaction of the rotor on the hub/controls due to the presence of the body, and the change in the interaction of the hub/controls on the rotor due to the presence of the body. If the assumption is made that the presence of the rotor does not change the interaction of the body on the hub/controls, and that the presence of the body does not change the mutual interaction between the rotor and hub/controls, then only the desired interaction

of the body on the rotor remains. However, this assumption may not be accurate.

In Ref. [9], it was assumed that the changes in these unmeasured interactions were small relative to the rotor forces and moments and that the interaction of the body on the rotor was valid. However, a closer examination of the sensitivity of rotor performance to small changes in measured drag indicates that this may not be true. At a free-stream dynamic pressure of 2.4 kPa ($\mu = 0.3$), the measured drag of the hub and controls with the rotor blades and body removed was about 100 N. When the body was present, the measured drag of the hub and controls was as much as 116 N, depending on the body position and angle of attack. Therefore, the interaction of the body on the hub/controls was as large as 16 N. It is expected that when the rotor is present, the interaction of the body on the hub/controls may be very different. This change would result in an undesired contribution to the interaction of the body on the rotor.

The rotor lift-to-drag ratio, used to indicate rotor performance, was calculated as follows:

$$\left(\frac{L}{D}\right)_R = \frac{L_R}{P/V - PF} \tag{3}$$

where L_R is the measured rotor lift, PF is the measured propulsive force, P is rotor power, and V is free-stream velocity. The denominator in the above equation represents the sum of the induced and profile drag of the rotor. The lift-to-drag ratio was used because it is a measure of the rotor efficiency. As the lift-to-drag ratio increases, power required for a given flight condition decreases. At an advance ratio of 0.3, a 10 N change in the measured propulsive force results in a 5% to 10% change in the lift-to-drag ratio, depending on the thrust level. The results shown in Ref. [9] indicate changes of about this magnitude, which were attributed to the effect of the body on the rotor. These results are now interpreted to be inconclusive. The uncertainty created by the interaction of the body on the hub and controls makes it impossible to determine the interaction of the body on the rotor alone. In addition, there are uncertainties in both the mutual interactions between the hub/controls and rotor and in the individual measurements of propulsive force, power, and lift, all of which affect lift-to-drag ratio. The interaction of the body on the rotor/hub combination is also of interest, but is not representative of a realistic configuration since the hub and controls were not properly scaled.

Since the hub forces cannot be separated from the rotor forces, the hub, controls, and rotor shaft should be accurately scaled such that there are no inappropriate forces being measured. This requires a scaled drive shaft extending from the body as it would in a real helicopter. A very accurate system for measuring rotor lift, propulsive force, and power is also required. These requirements may be difficult to achieve at model scale. Model hubs designed for full-scale tip speeds tend to be oversized due to structural requirements. An internal balance system for the rotor forces and moments may provide more accuracy than the 7- by 10-Foot Wind Tunnel balance system,

particularly for rotor power. Even so, this approaach may not be accurate enough, and the problem of a scaled hub remains. Therefore, it is suggested that full-scale testing may be the best approach to obtain these measurements.

5. Future Plans

A full-scale investigation of rotor/body interactions in the Ames 40- by 80-Foot Wind Tunnel is currently being planned. The full-scale version of body B_2 will be tested with a four-bladed rotor system. The body configuration will be varied by adding an extension to the forward part, simulating a typical helicopter. This extended nose will be installed in two vertical positions, simulating a change in rotor height. The body shell will be supported on load cells providing measurements of the body forces and moments. The wind-tunnel balance system will measure the total rotor and body forces and moments. Rotor torque will be determined from shaft strain gages, and body surface pressure measurements will also be obtained.

Since the hub and controls will be full scale, some of the problems described above will be avoided. Because of the larger loads, the data should be more accurate than those obtained in the 7- by 10-Foot Wind Tunnel. However, it will remain impossible to separate the hub loads from the rotor loads. Because the body provides the support and drive system for the rotor, it will not be possible to determine the total interference of the body on the rotor performance by completely removing the body. However, changes in performance of the rotor/hub combination will be determined for changes in the body geometry and position. It is expected that this investigation will provide high-quality measurements of the mutual interactions occurring in a full-scale rotor/body system.

This test will also include a tail rotor mounted on an independent stand which is capable of varying the tail rotor position. This will provide aerodynamic and acoustic data on main rotor/tail rotor interactions as well as on the effects of the tail rotor on the rotor/body interactions.

A new small-scale rotor rig incorporating a four-bladed rotor and an internal rotor balance system has been acquired. Investigations of rotor/body interactions and rotor/wing interactions will be pursued with this system in both the Ames 7- by 10-Foot Wind Tunnel and in hover. By placing the body around the drive shaft, a more representative configuration will be obtained. The internal rotor balance will provide measurements only of the loads on the components not enclosed by the body, i.e., the rotor, hub, and shaft. The hub and shaft will remain somewhat oversized, but will be more representative of a real helicopter system.

6. Conclusions

1) The presence of a hub and rotor causes large changes in body lift, drag, and pitching moment. For a body of revolution, lift and drag increase while the pitching moment change is negative.

2) The effect of the hub on the body is very significant, particularly at high speed, and should be included in analytical techniques for predicting rotor/body interactions.

3) Body forces and moments vary with both free-stream dynamic pressure and rotor thrust. Body lift, drag, and pitching moment, normalized by rotor thrust, can be approximated by a linear function of the ratio of free-stream dynamic pressure to rotor disk loading for a given body angle of attack, rotor tip-path-plane angle, and rotor/body position.

4) As the rotor tip-path plane is tilted forward from 0° to 8°, body lift increases and body pitching moment shifts negatively.

5) Increases in vertical separation between the rotor and body are accompanied by a body lift decrease and a positive shift in body pitching moment.

6) The presence of the hub with rotor blades off produces changes in body lift, drag, and pitching moment proportional to the free-stream dynamic pressure; lift and drag increase while there is a negative change in pitching moment.

7) The hub and rotor interference effects on the body vary with body angle of attack; hub interference may be responsible for a major part of the trend.

8) Large changes in body lift, drag, and pitching moment occur when the body longitudinal position relative to the rotor is varied; the hub interference may be responsible for a major part of the trend.

9) An appropriately scaled hub and control system are required to determine interaction effects of a body on rotor system performance. Full-scale testing may be the best approach to obtain these data.

10) Rotor/body interactions must be considered when determining rotor performance from wind-tunnel tests even when a body of revolution is used as the test module.

References

1) P. F. Sheridan, Interactional Aerodynamics of the Single Rotor Helicopter Configuration, U.S. Army Research and Technology Laboratories TR-78-23, Sept. 1978.

2) P. F. Sheridan and R. P. Smith, Interactional Aerodynamics — A New Challenge to Helicopter Technology, Journal of the American Helicopter Society, Vol. 25, No. 1, Jan. 1980, pp. 3-21.

3) John C. Wilson and Raymond E. Mineck, Wind Tunnel Investigation of Helicopter-Rotor Wake Effects on Three Helicopter Fuselage Models, NASA TM X-3185, 1975.

4) Carl E. Freeman and Raymond E. Mineck, Fuselage Surface Pressure Measurements of a Helicopter Wind-Tunnel Model With a 3.15-Meter Diameter Single Rotor, NASA TM-80051, 1979.

5) Carl E. Freeman and John C. Wilson, Rotor-Body Interference (ROBIN) -- Analysis and Test, Paper No. 80-5, 36th Annual Forum of the American Helicopter Society, Washington, D.C., May 1980.

6) P. G. Wilby, C. Young, and J. Grant, An Investigation of the Influence of Fuselage Flow Field on Rotor Loads and the Effects of Vehicle Configuration, Vertica, Vol. 3, 1979, pp. 79-94.

7) Ross P. Menger, Tommie L. Wood, and John T. Brieger, Effects of Aerodynamic Interaction Between Main and Tail Rotors on Helicopter Hover Performance and Noise, NASA CR-166477, Feb. 1983.

8) D. T. Balch, An Experimental Study of Main Rotor/Tail Rotor/Airframe Interactions in Hover, 39th Annual Forum of the American Helicopter Society, St. Louis, Mo., May 1983.

9) M. D. Betzina and P. S. Shinoda, Aerodynamic Interactions Between a 1/6-Scale Helicopter Rotor and a Body of Revolution, NASA TM-84247, June 1982.

10) Charles A. Smith and Mark D. Betzina, A Study of the Aerodynamic Interaction Between a Main Rotor and a Fuselage, Paper No. 83-39-73, 39th Annual Forum of the American Helicopter Society, St. Louis, Mo., May 1983.

11) P. Shinoda and D. Signor, An Experimental Investigation of the Aerodynamic Interactions between a Helicopter Rotor and a Body of Revolution, NASA TM to be published.

12) A. Pope and J. J. Harper, Low-Speed Wind Tunnel Testing, John Wiley & Son, Inc., 1966, pp. 327-332.

TABLE 1.- ROTOR GEOMETRY

Parameter	Value
Number of blades, b	2
Rotor radius, R	1.118 m
Blade chord, c	0.114 m
Rotor solidity, $bc/\pi R$	0.0651
Blade precone angle	1.33°
Blade twist (linear)	-10°
Blade taper ratio	1.0
Airfoil	modified NACA 0012
Flapping hinge underslung	0.0091 m
Blade Lock number	3.44

TABLE 2.- TEST PARAMETERS

Parameter	Body B_1	Body B_2	Body B_2E
Advance ratio, m	0.10	0.15	0.15
	0.20	0.20	0.20
	0.30	0.25	0.25
		0.30	0.30
Rotor tip Mach number	0.60	0.60	0.60
Body angle of attack α_B, deg	0	4	0
	-4	0	
	-8	-4	
Tip-path-plane angle of attack, α_{TPP}, deg	0	0	0
	-4	-4	-4
	-8	-8	-8
Thrust-coefficient-to-solidity ratio, C_T/σ	0.03-0.10	0.03-0.10	0.03-0.10
Rotor/body vertical separation, Z/R	0.213*	0.215	0.229
	0.235	0.229*	
		0.245	
		0.260	
		0.275	
Rotor/body longitudinal position, X/R	0.447*	0.203*	0.481
	0.538	0.481	

*Baseline position.

TABLE 3.- BALANCE MEASUREMENTS

Configuration			Balance measurement	
Body	Hub	Rotor	Wind tunnel	Body
X			--	B
X	X		H + H/B	B + B/H
X	X	X	HR + HR/B	B + B/HR
	X	X	HR	--
	X		H	--

B = body
H = hub and controls
R = rotor
x/y = interference on component x due to presence of component y
HR = H + R + H/R + R/H

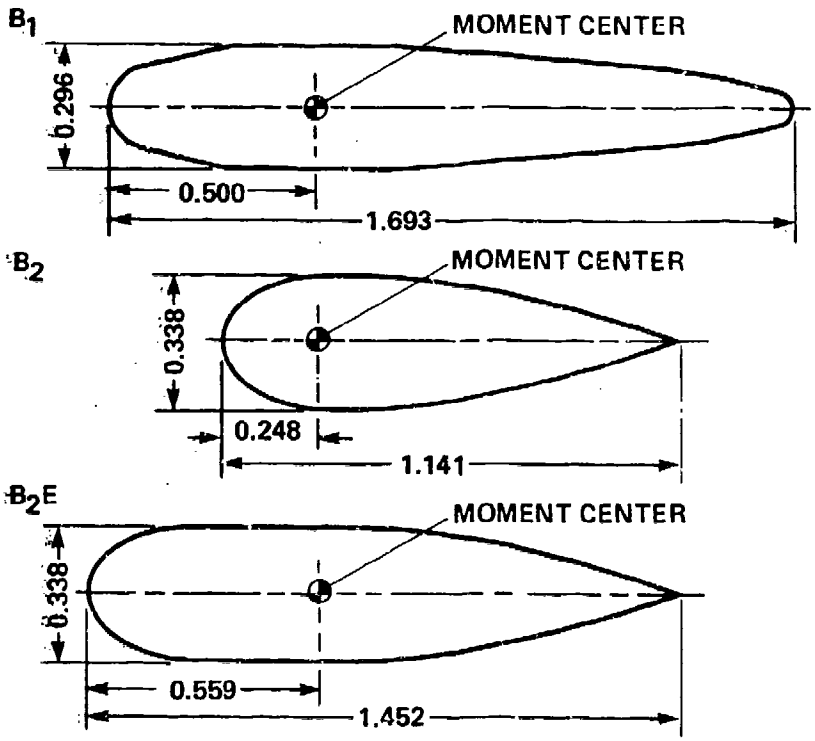

NOTE: ALL BODIES ARE CIRCULAR IN CROSS SECTION
ALL DIMENSIONS ARE IN meters

Fig. 1. Bodies of revolution.

Fig. 2. Full-scale rotor test apparatus in the Ames 40- by 80-Foot Wind Tunnel.

Fig. 3. Model installation in the Ames 7- by 10-Foot Wind Tunnel.

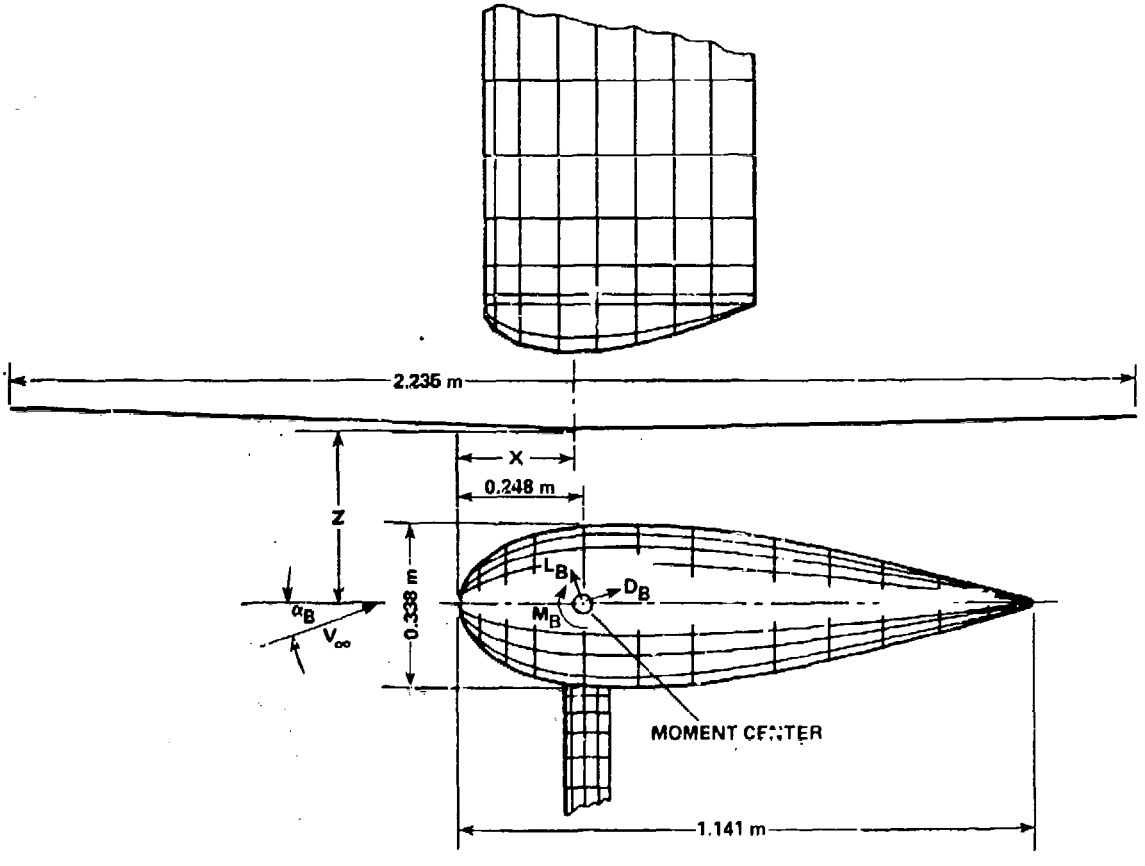

Fig. 4. Model schematic.

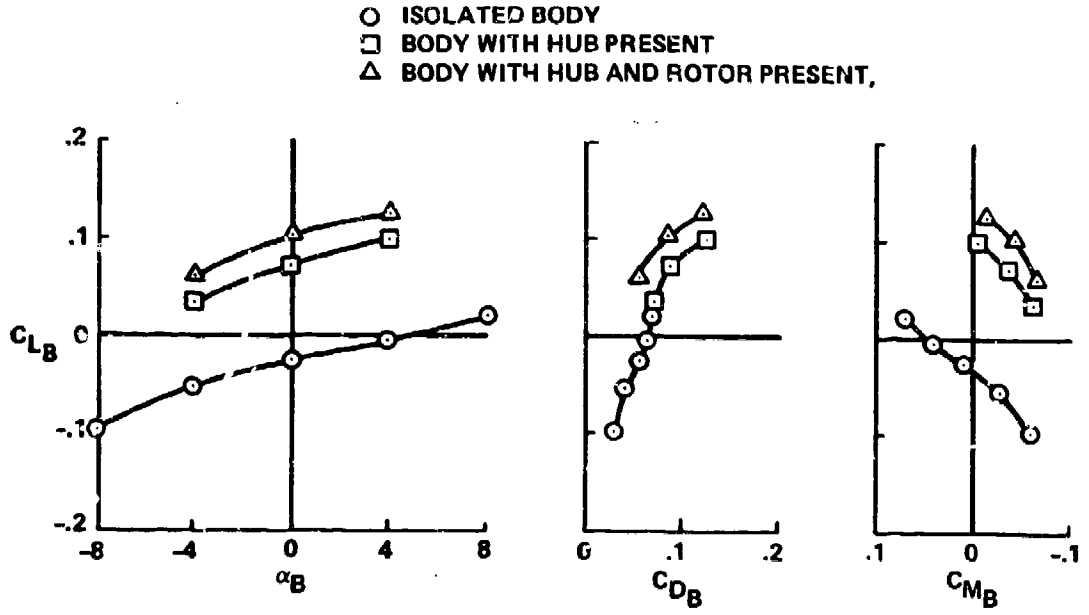

Fig. 5. Interference effect of hub and rotor on body B_2 longitudinal characteristics; baseline position, V = 61 m/sec, μ = 0.3, α_{TPP} = 0°, C_T = 0.00408.

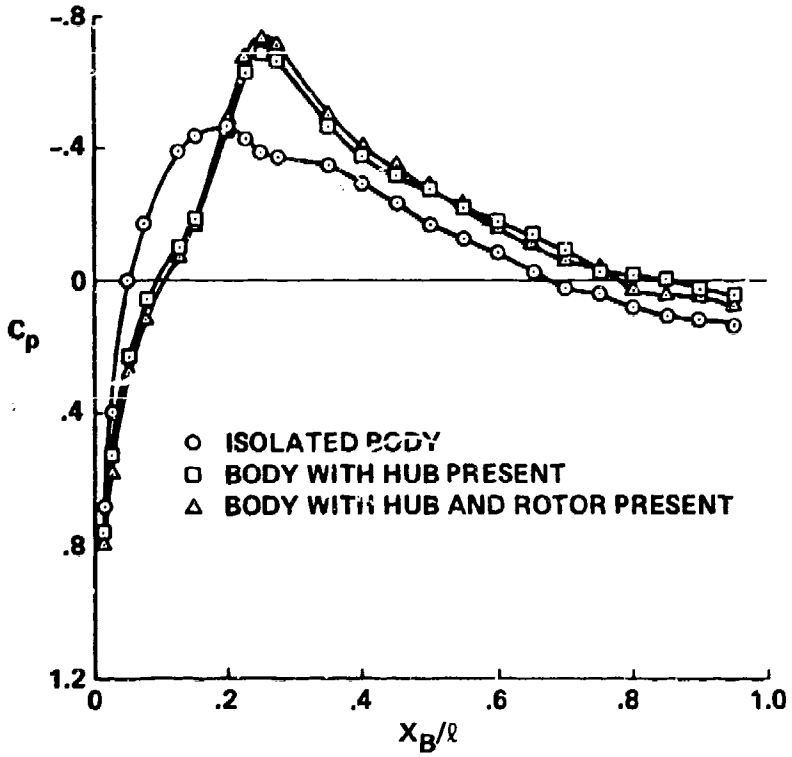

Fig. 6. Interference effect of hub and rotor on body B_2 upper surface pressure distribution; baseline position, α_B = 0°, V = 61 m/sec, μ = 0.3, α_{TPP} = 0°, C_T = 0.00408.

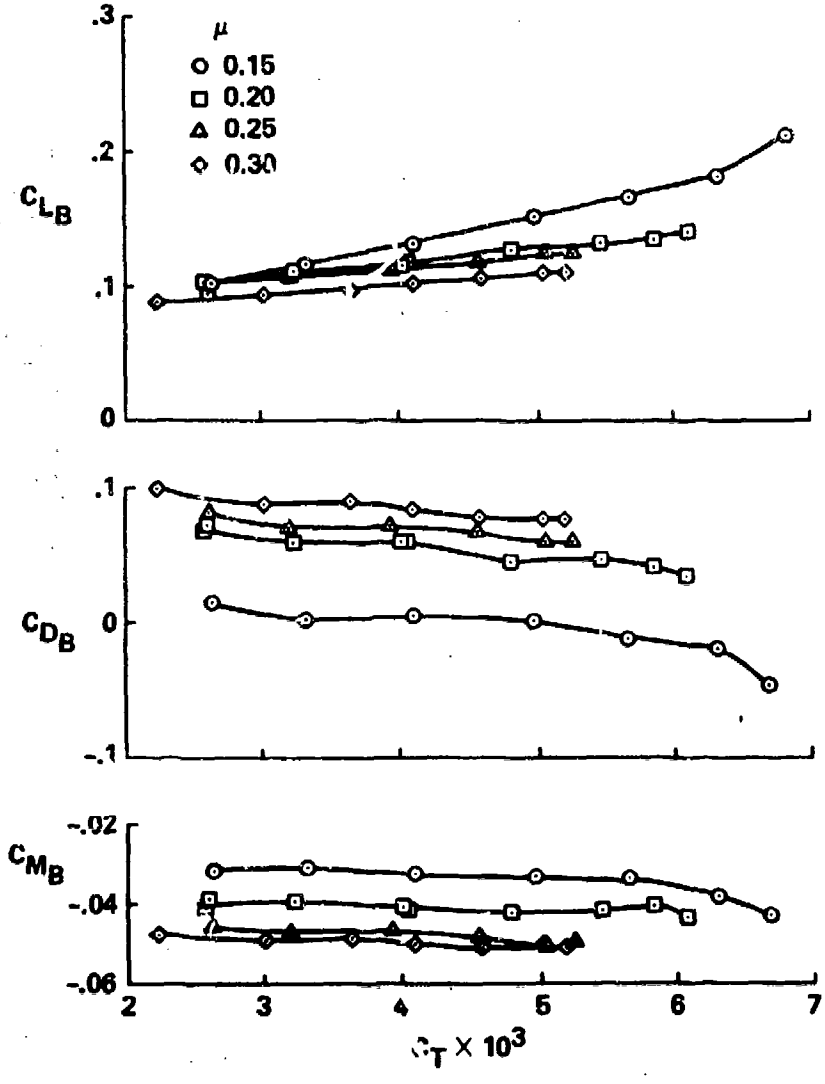

Fig. 7. Effect of rotor thrust on body B_2 longitudinal characteristics; baseline position, $\alpha_B = 0°$, $\alpha_{TPP} = 0°$.

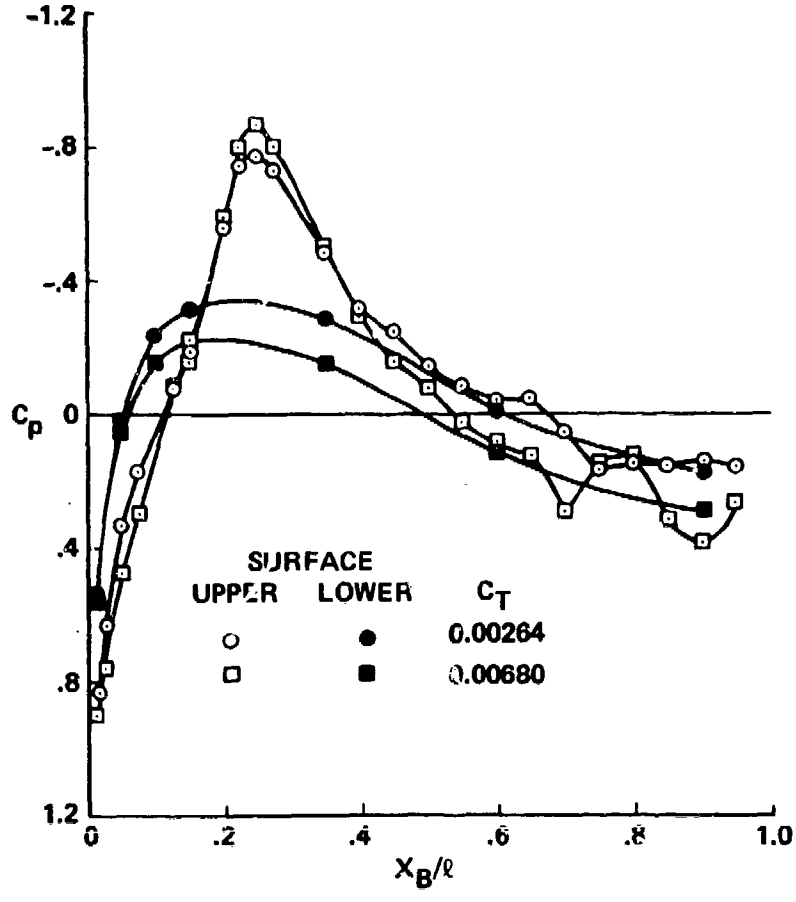

Fig. 8. Effect of rotor thrust on body B_2 surface pressure distribution; baseline position, $\alpha_B = 0°$, $\alpha_{TPP} = 0°$, $\mu = 0.15$.

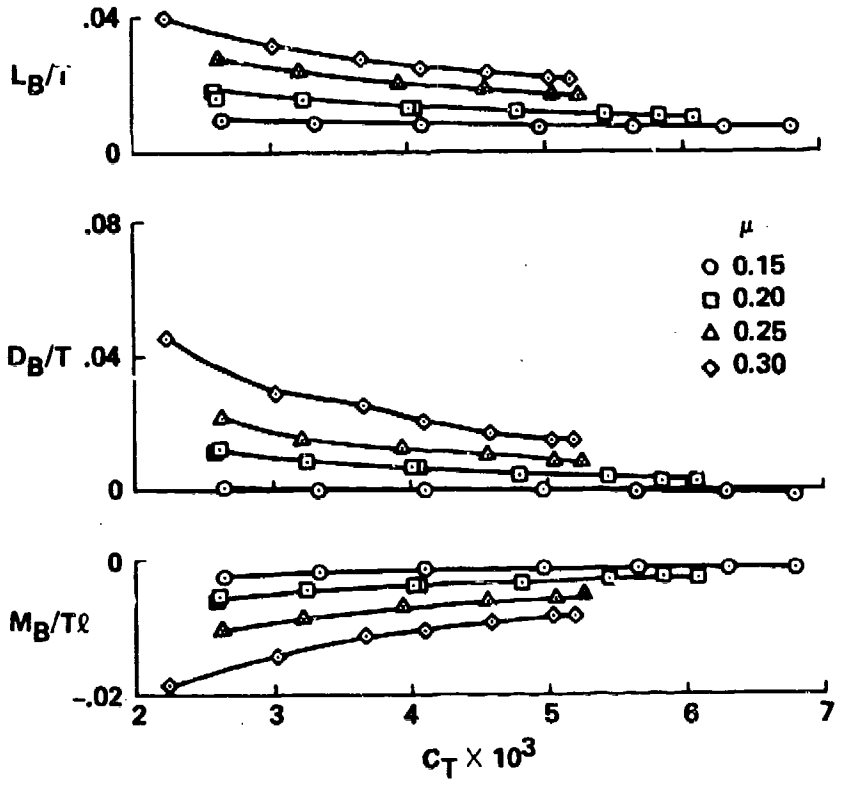

Fig. 9. Variation of body B_2 longitudinal characteristics with rotor thrust and advance ratio; baseline position, $\alpha_B = 0°$, $\alpha_{TPP} = 0°$.

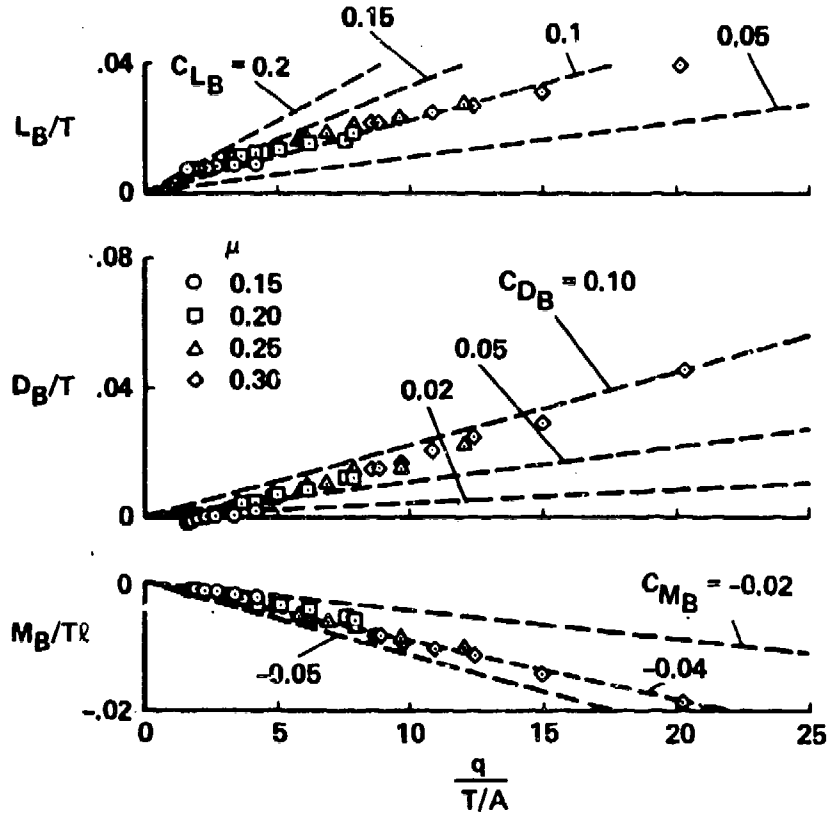

Fig. 10. Variation of body B_2 longitudinal characteristics with ratio of free-stream dynamic pressure to rotor disk loading; baseline position, $\alpha_B = 0°$, $\alpha_{TPP} = 0°$.

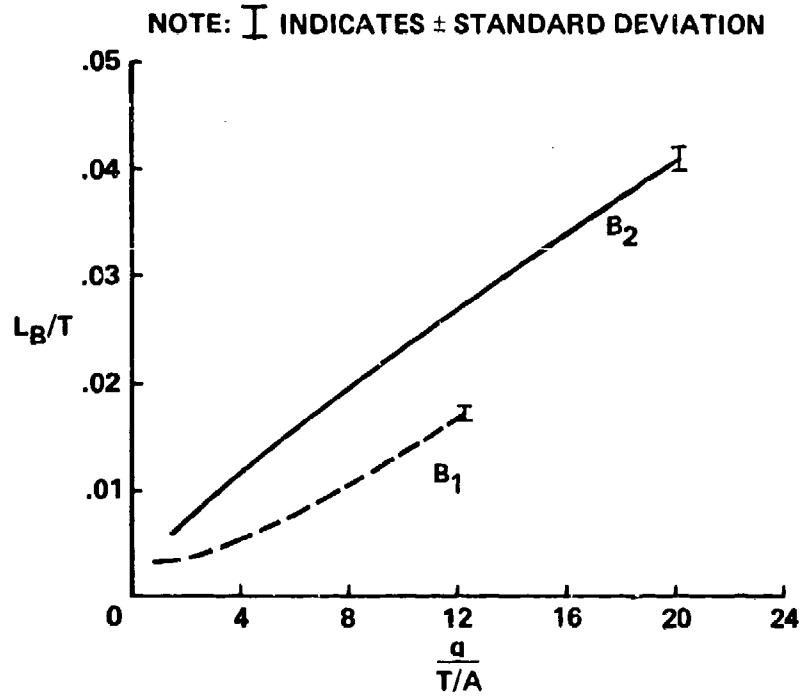

Fig. 11. Effect of body configuration on body lift; baseline positions, $\alpha_B = 0°$, $\alpha_{TPP} = 0°$.

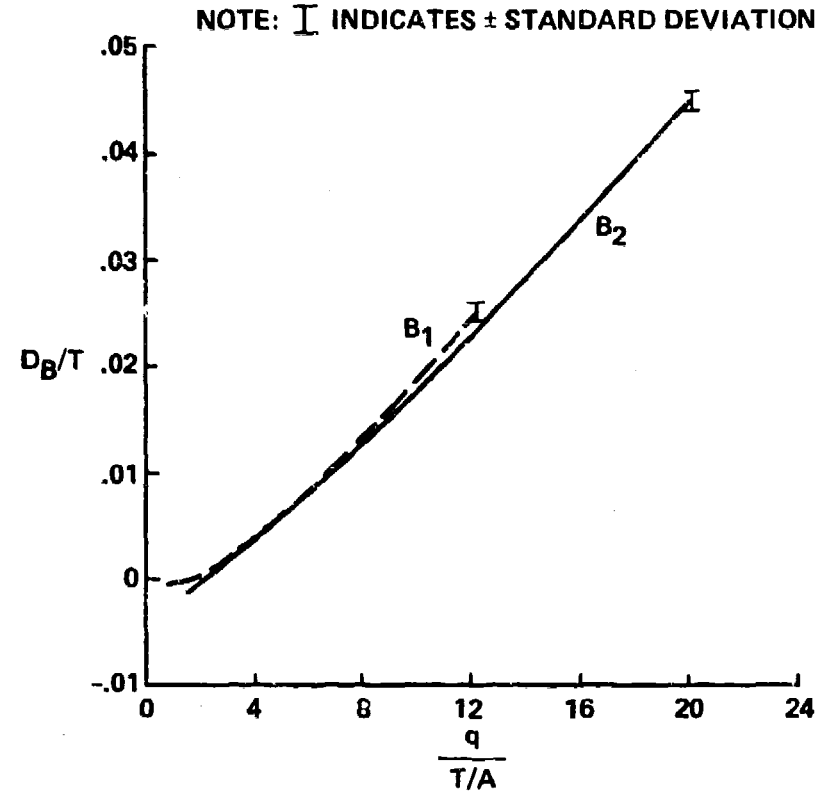

Fig. 12. Effect of body configuration on body drag; baseline positions, $\alpha_B = 0°$, $\alpha_{TPP} = 0°$.

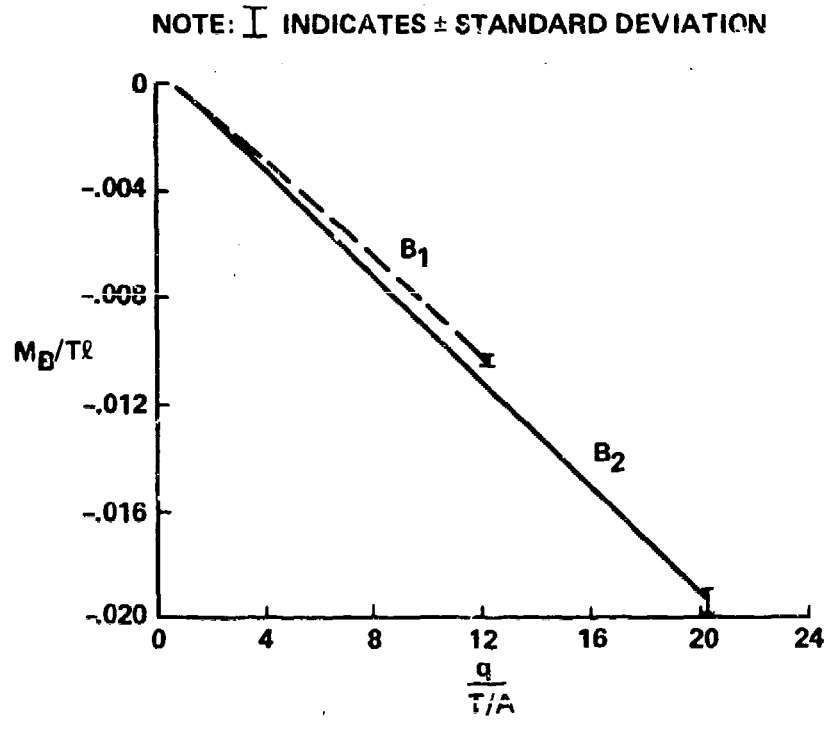

Fig. 13. Effect of body configuration on body pitching moment; baseline positions, $\alpha_B = 0°$, $\alpha_{TPP} = 0°$.

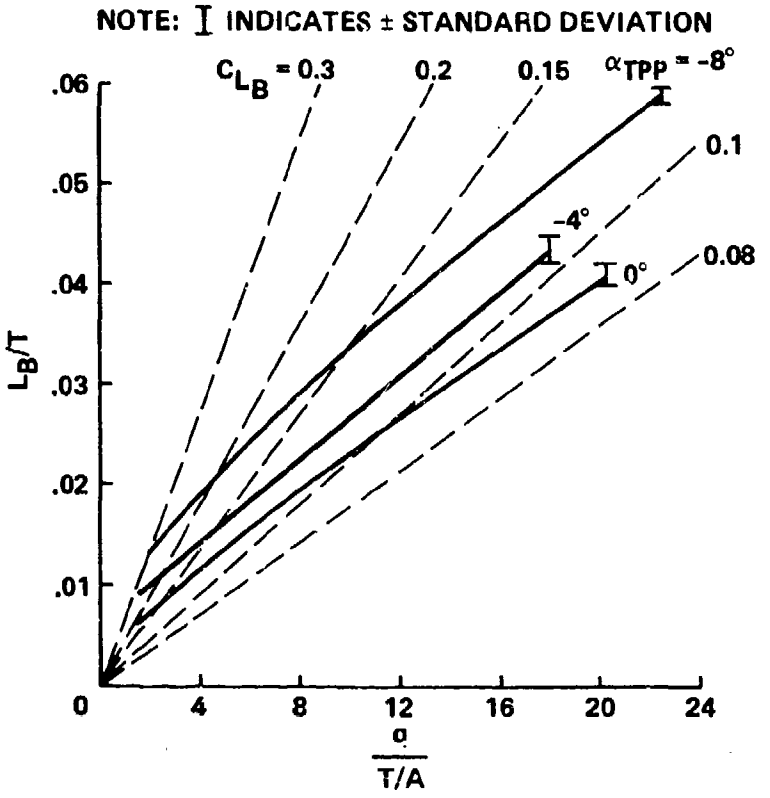

Fig. 14. Effect of rotor tip-path-plane angle on body B_2 lift, baseline position, $\alpha_B = 0°$.

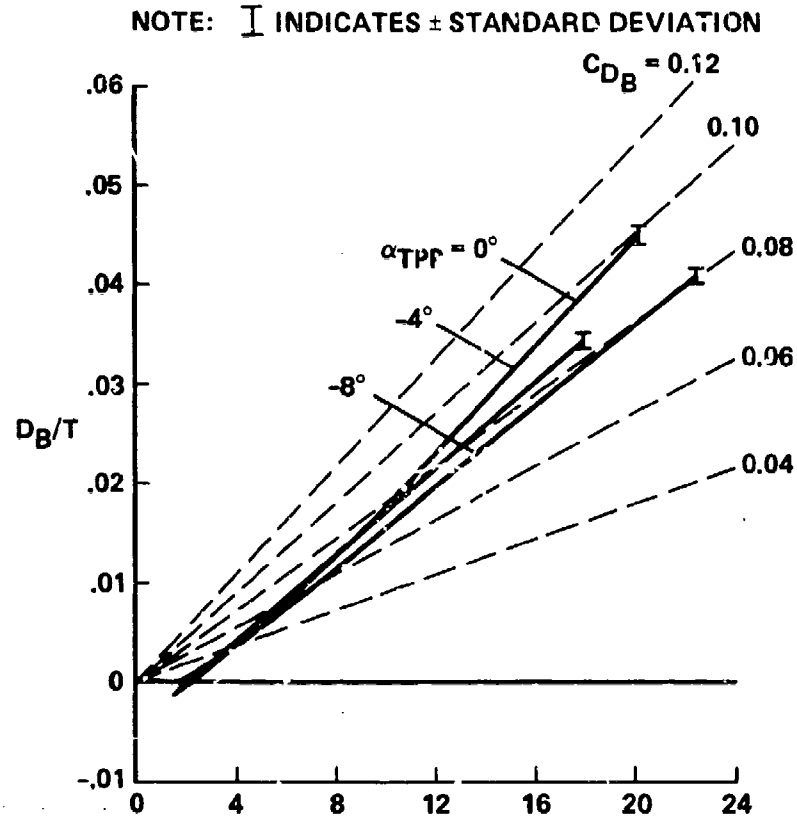

Fig. 15. Effect of rotor tip-path-plane angle on body B_2 drag; baseline position, $\alpha_B = 0°$.

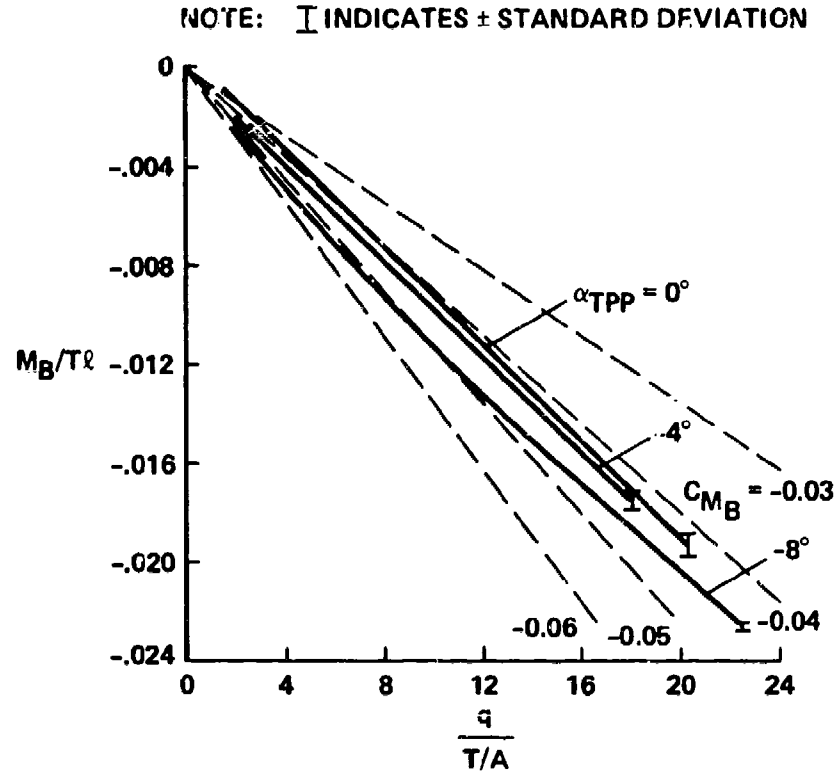

Fig. 16. Effect of rotor tip-path-plane angle on body B_2 pitching moment; baseline position, $\alpha_B = 0°$.

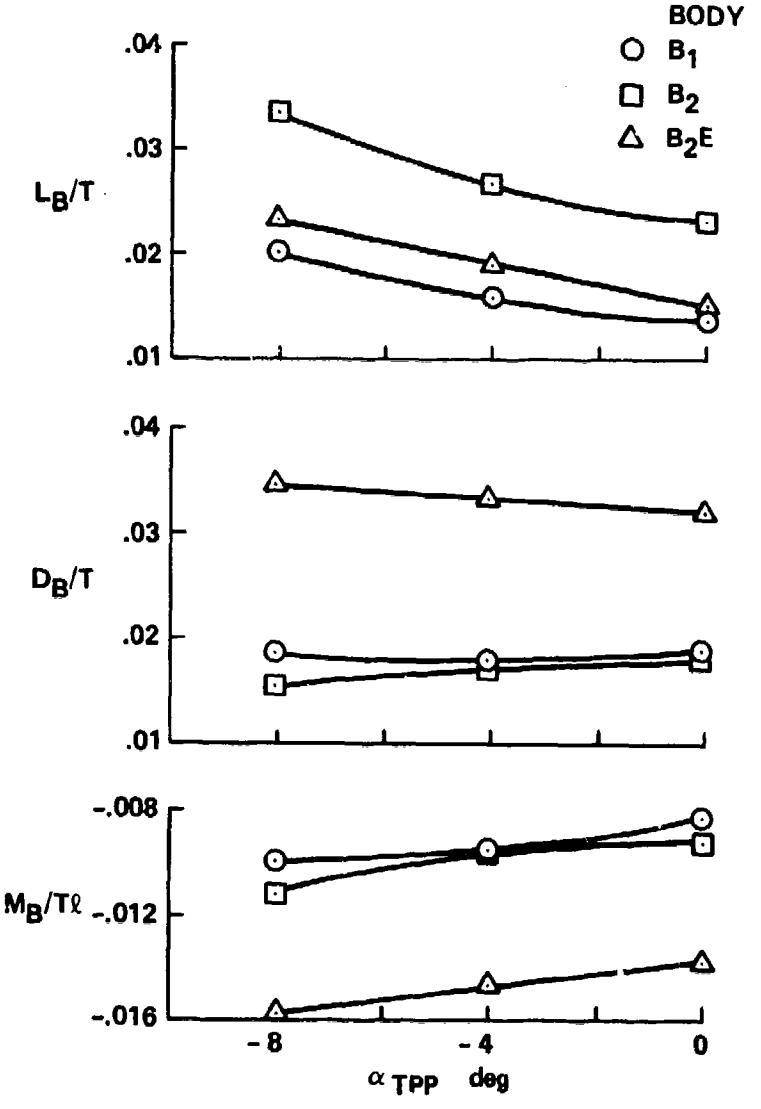

Fig. 17. Effect of rotor tip-path-plane angle on various bodies; baseline positions, $\alpha_B = 0°$, $q/(T/A) = 10$.

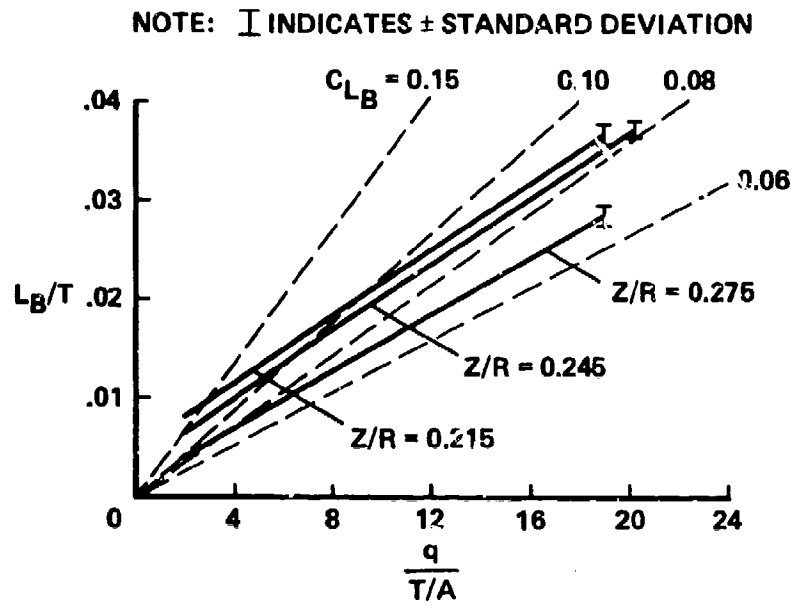

Fig. 18. Effect of vertical separation on body B_2 lift; $\alpha_B = 0°$, $\alpha_{TPP} = 0°$, X/R = 0.203.

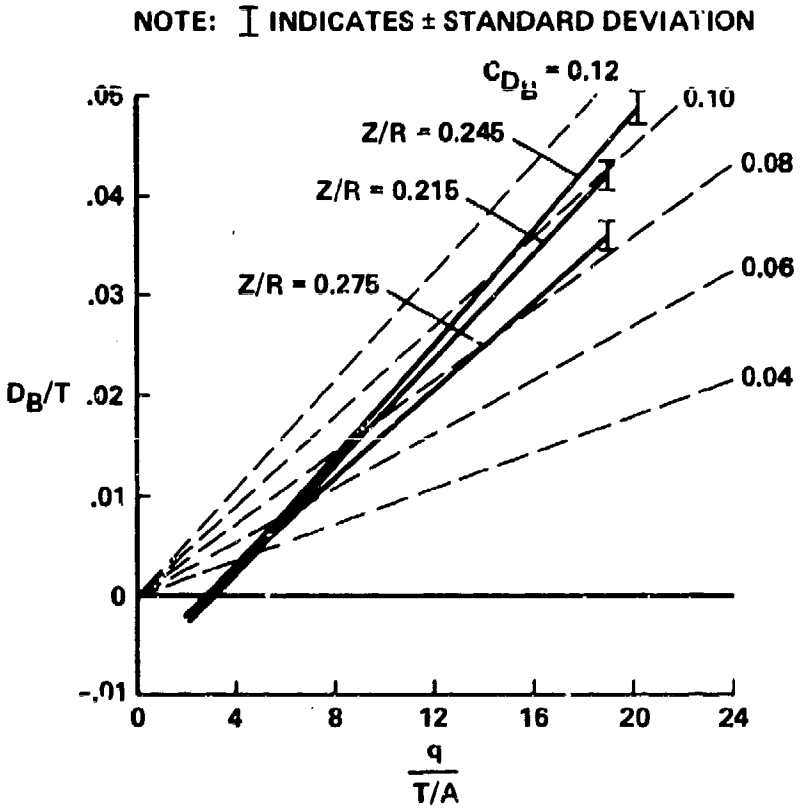

Fig. 19. Effect of vertical separation on body B_2 drag; $\alpha_B = 0°$, $\alpha_{TPP} = 0°$, X/R = 0.203.

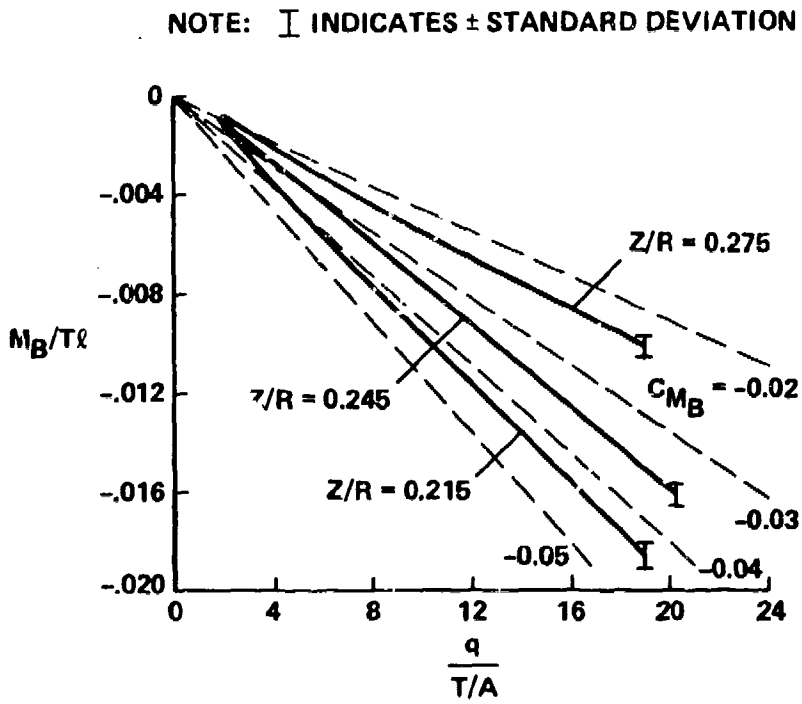

Fig. 20. Effect of vertical separation on body B_2 pitching moment; α_B = C°, α_{TPP} = 0°, X/R = 0.203.

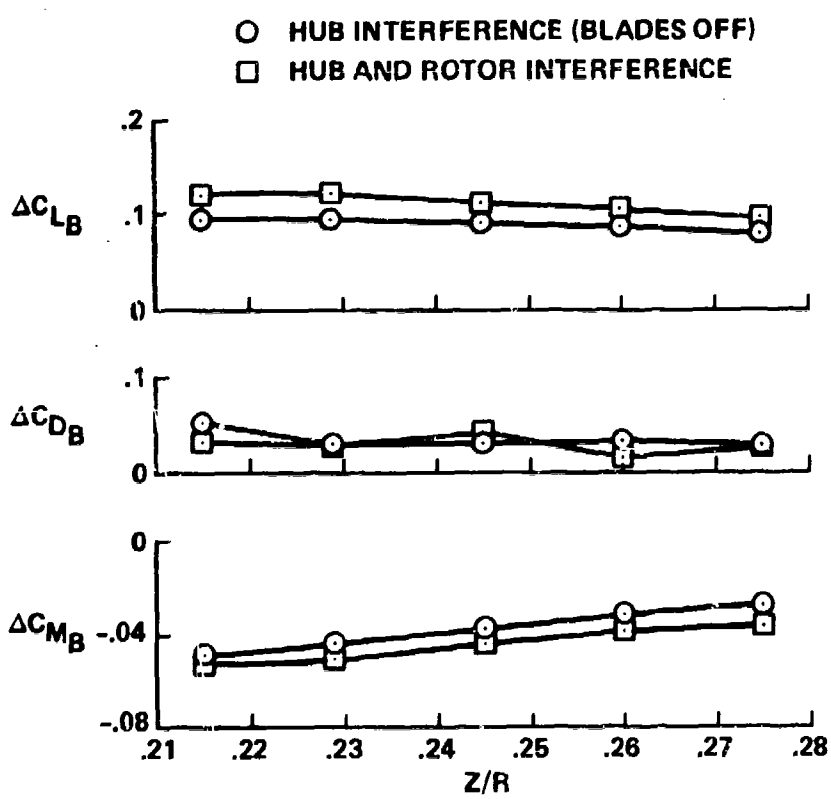

Fig. 21. Effect of vertical separation on hub and rotor interference on body B_2; α_B = 0°, α_{TPP} = 0°, X/R = 0.203, V = 60 m/sec, μ = 0.30, C_T = 0.0039.

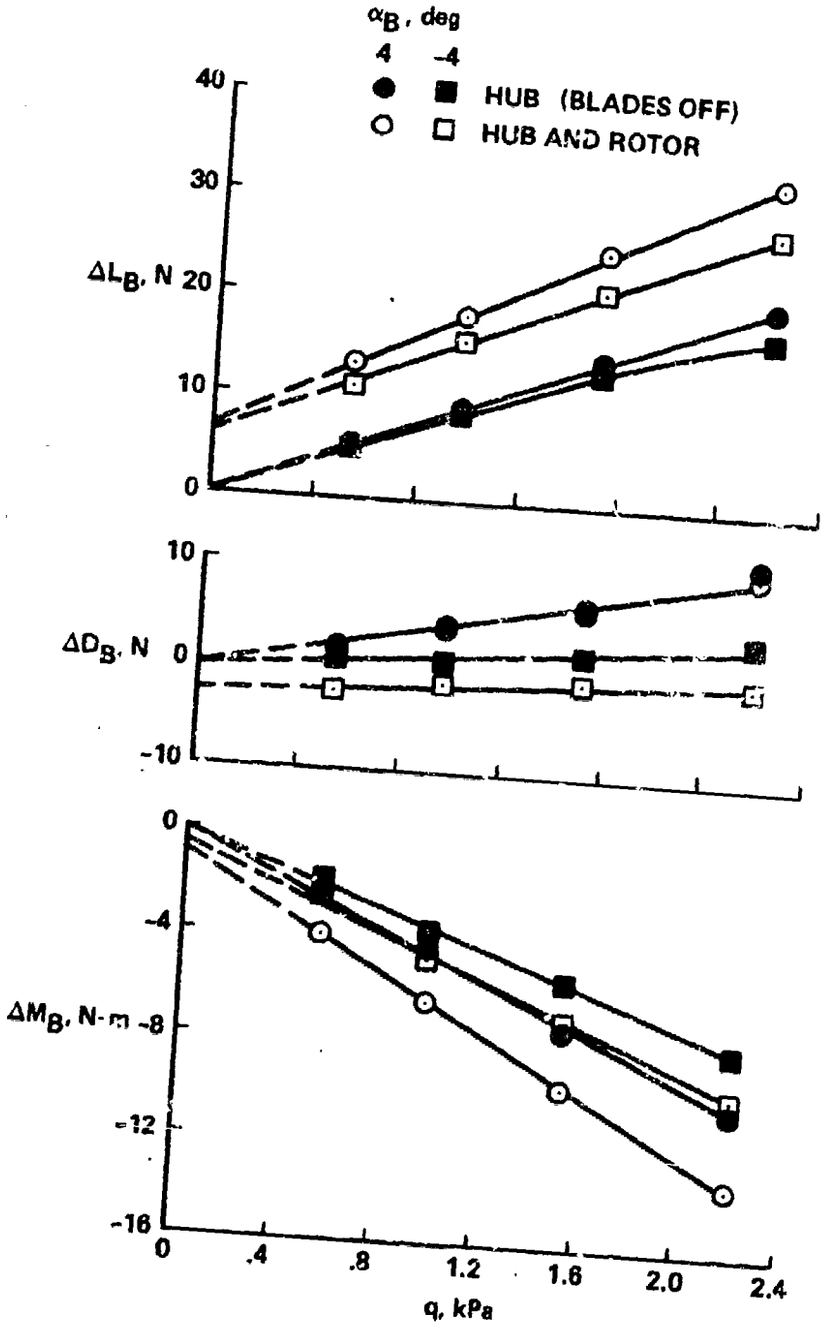

Fig. 22. Hub and rotor interference effects on body B_2; baseline position, $\alpha_{TPP} = -8°$, $C_T = 0.0039$.

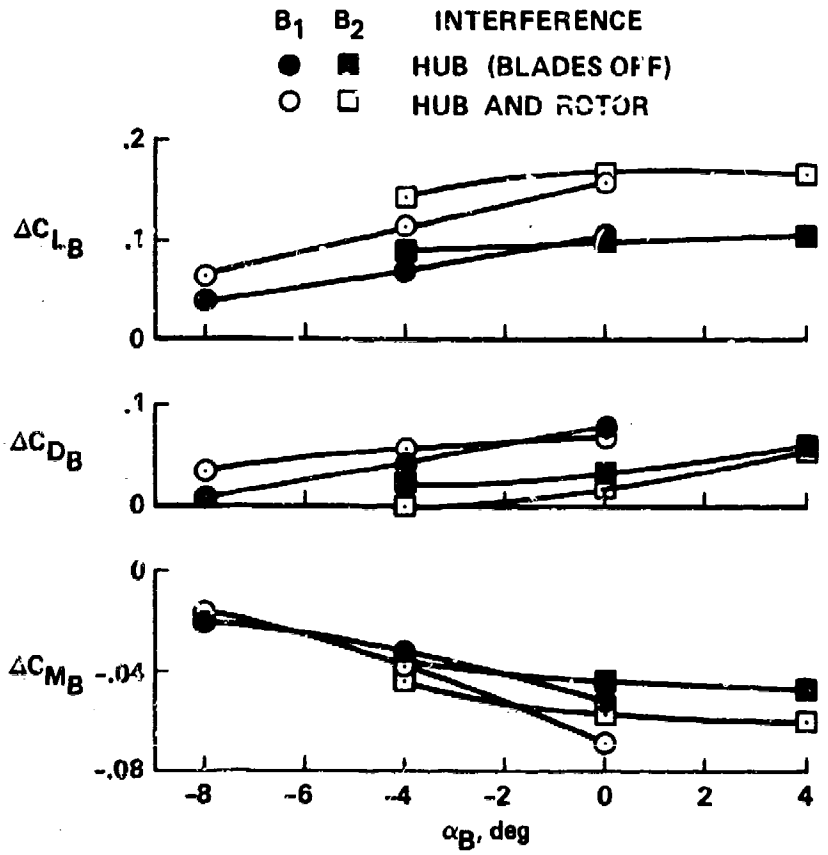

Fig. 23. Effect of body angle of attack on hub and rotor interference: baseline position, $\alpha_{TPP} = 0°$, V = 60 m/sec, $\mu = 0.30$, $C_T = 0.0039$.

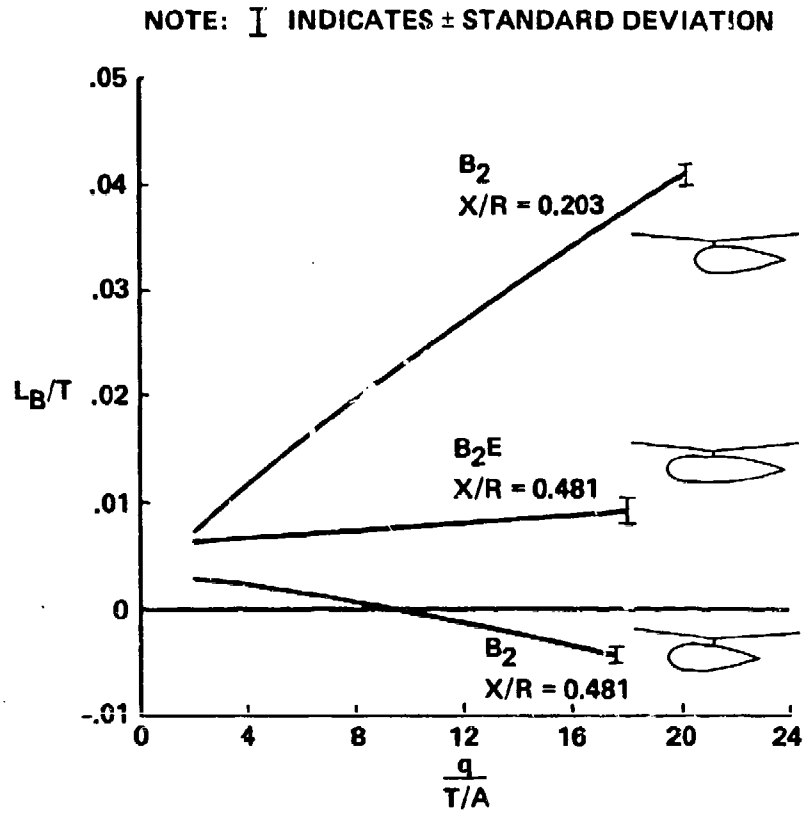

Fig. 24. Effect of body longitudinal position on body lift; $\alpha_B = 0°$, $\alpha_{TPP} = 0°$, Z/R = 0.229.

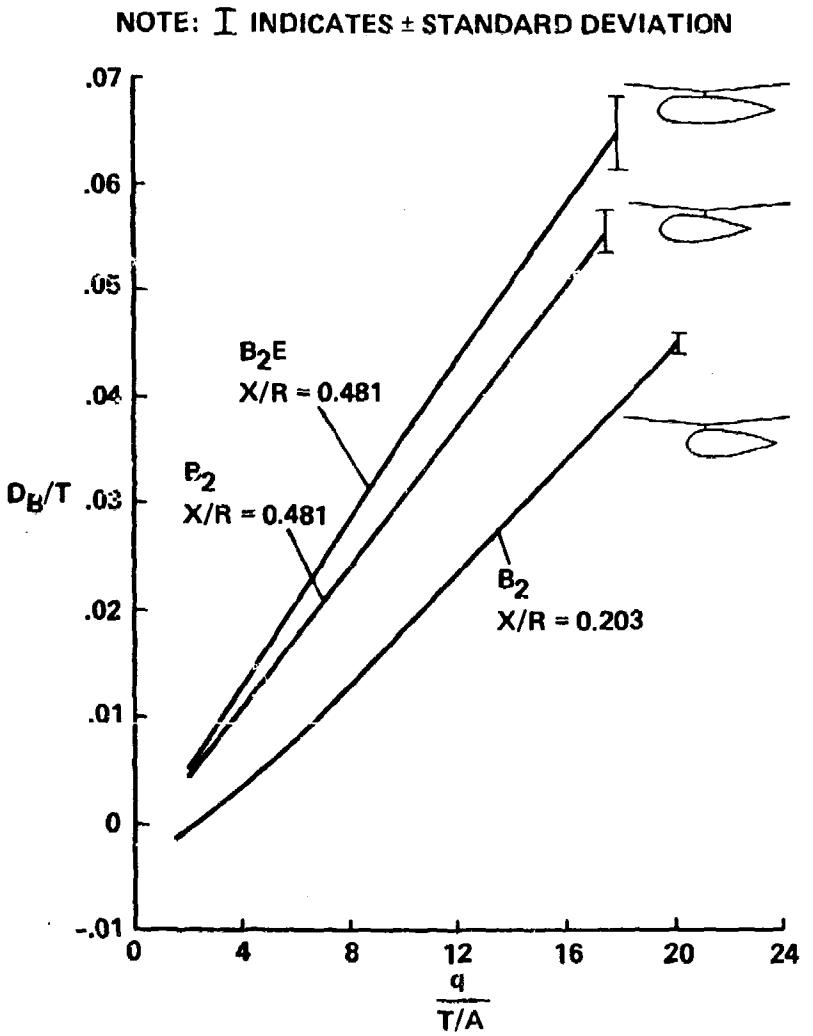

Fig. 25. Effect of body longitudinal position on body drag; $\alpha_B = 0°$, $\alpha_{TPP} = 0°$, Z/R = 0.229.

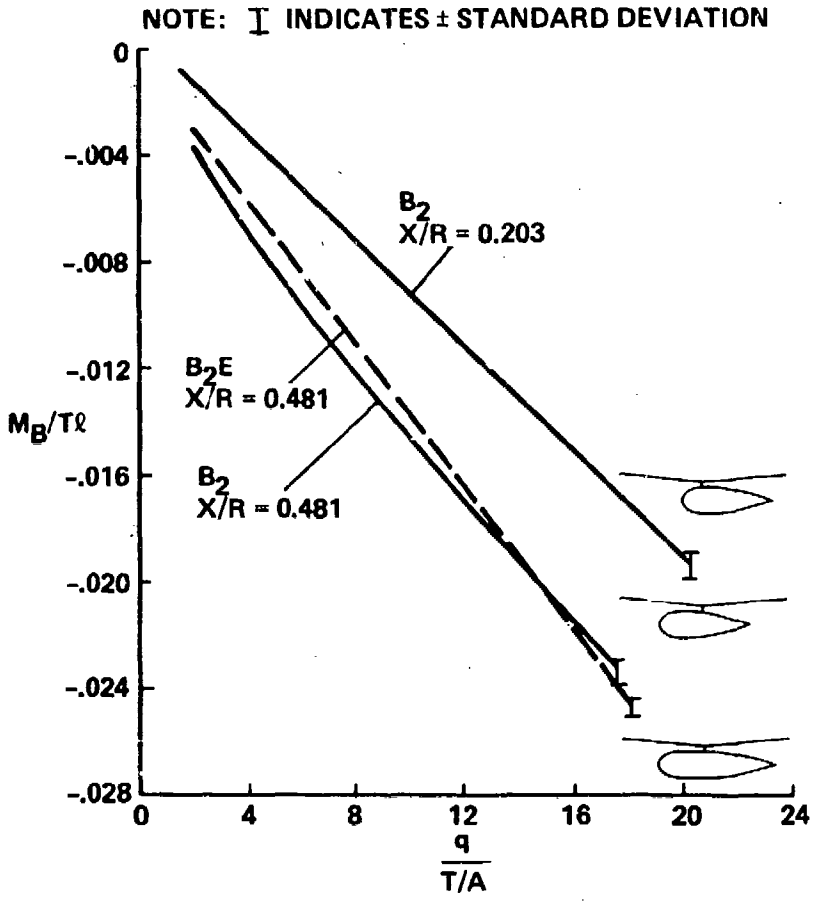

Fig. 26. Effect of body longitudinal position on body pitching moment; $\alpha_B = 0°$, $\alpha_{TPP} = 0°$, Z/R = 0.229.

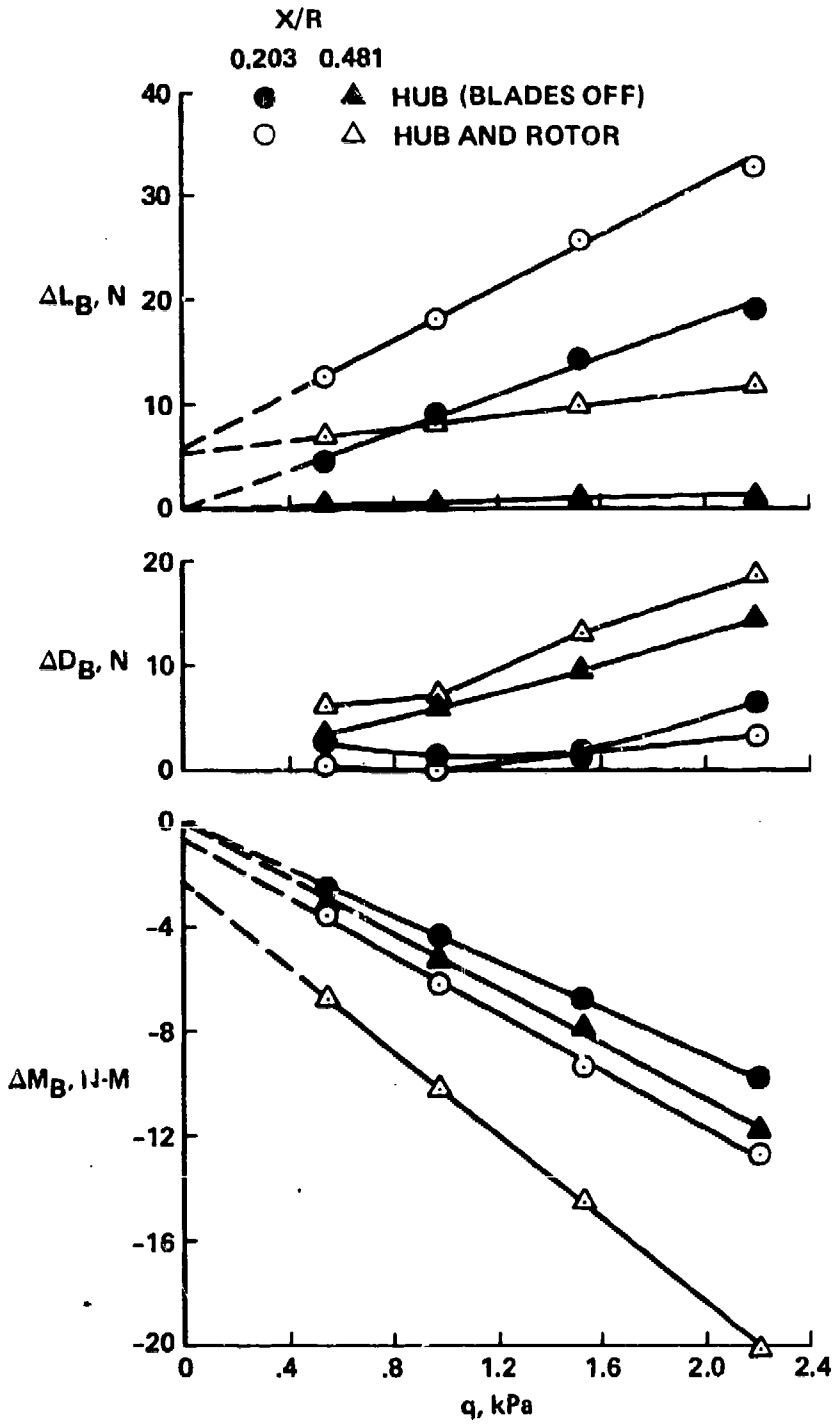

Fig. 27. Effect of body B_2 longitudinal position on hub and rotor interference; $\alpha_B = 0°$, $\alpha_{TPP} = -8°$, $Z/R = 0.229$, $C_T = 0.0039$.

1. Report No.	2. Government Accession No.	3. Recipient's Catalog No.
NASA TM 85844	AD-A135040	

4. Title and Subtitle	5. Report Date
ROTOR/BODY AERODYNAMIC INTERACTIONS	October 1983
	6. Performing Organization Code

7. Author(s)	8. Performing Organization Report No.
Mark D. Betzina, Charles A. Smith and Patrick Shinoda*	A-9500
	10. Work Unit No. T 5485A
9. Performing Organization Name and Address Ames Research Center, Moffett Field, CA. *Aeromechanics Laboratory, Research and Technology Laboratories, US Army Aviation Research & Development Command, Ames Research Center, Moffett Field, CA.	11. Contract or Grant No.
	13. Type of Report and Period Covered Technical Memorandum
12. Sponsoring Agency Name and Address National Aeronautics and Space Administration Washington, DC, 20546 and US Army Aviation R&C Command, St. Louis, MO 93166	14. Sponsoring Agency Code 505-42-11

15. Supplementary Notes

Point of contact: Mark Betzina, NASA, Ames Research Center, Moffett Field, California 94035 (415) 965-6679 or FTS 448 6679

16. Abstract

A wind-tunnel investigation was conducted in which independent, steady-state aerodynamic forces and moments were measured on a 2.24-m-diam. two-bladed helicopter rotor and on several different bodies. The objective was to determine the mutual interaction effects for variations in velocity, thrust, tip-path-plane angle of attack, body angle of attack, rotor/body position, and body geometry. The results of the investigation show that the body longitudinal aerodynamic characteristics are significantly affected by the presence of a rotor and hub, and that the hub interference may be a major part of such interaction. This report presents the effects of the body on the rotor performance. Also discussed are plans for future research into this subject.

17. Key Words (Suggested by Author(s))	18. Distribution Statement
Helicopter Rotor Aerodynamic interactions Rotor/body interactions	Unlimited Subject Category:02

19. Security Classif. (of this report)	20. Security Classif. (of this page)	21. No. of Pages	22. Price*
Uncl	Uncl	39	A02

*For sale by the National Technical Information Service, Springfield, Virginia 22161